AIAA SciTech Forum
23-27 January 2023, National Harbor, MD & Online
AIAA SCITECH 2023 Forum

10.2514/6.2023-2281

Scaling of Hovering Rotorcraft Aerodynamics in Hyperbaric Experimental Conditions

Constantinos S. Kandias* and Mark A. Miller†
Pennsylvania State University, State College, PA, 16801, USA

This paper analyzes the ability to experimentally measure the aerodynamic performance of rotorcraft blades using small-scale models. If the model scale is reduced significantly enough relative to the full scale vehicle rotor, the nature of the aerodynamic phenomena involved changes drastically, which can significantly alter the overall rotor performance. This stems from the inherent dependence of airfoil performance on Reynolds number, and the inability to keep both Reynolds number and Mach number constant for a scaled rotor under normal atmospheric conditions. By conducting experiments in a hyperbaric chamber, density can be controlled as an additional experimental parameter allowing for better replication of full-scale operating conditions and aerodynamic behavior. Experiments can therefore be conducted using smaller models, better facilitating low-cost, high-fidelity measurements of the complex aerodynamics at play in rotorcraft applications. Performance data from a 1/8th scale model of an Urban Air Mobility (UAM) type rotor is presented to illustrate the dependence of performance on Reynolds number. A UAM rotor was chosen due to the potential applicability of this technique to investigate interactional effects of multirotor systems. Although the present paper focuses only on an isolated rotor operating in hover, the results of this study will be used to inform future work on multirotor systems, such as tandem and coaxial rotor configurations, investigating the interactions between the individual rotors and their wakes. The results quantify the behavior of the rotor over a wide range of equivalent scales, clearly displaying a sharp degradation in performance for low Reynolds numbers, below approximately $Re = 100,000$. This performance decrease can be linked to the dependence of airfoil C_l and C_d on Reynolds number, outlining the need to accurately replicate full-scale Reynolds numbers in an experimental model, and the ability for high-pressure aerodynamic testing to facilitate such investigations at low cost relative to a full-scale experimental study.

I. Nomenclature

A	=	rotor disk area
a	=	sonic velocity
C_d	=	drag coefficient
C_l	=	lift coefficient
C_P	=	rotor power coefficient
C_T	=	rotor thrust coefficient
c	=	airfoil chord
dD	=	blade element drag
dL	=	blade element lift
dP	=	blade element power
dQ	=	blade element torque
dT	=	blade element thrust
M	=	Mach number
R	=	rotor radius
r	=	blade element radial location
Δr	=	blade element radial width
Re	=	Reynolds number

*Graduate Research Assistant, Aerospace Engineering, 229 Hammond Building, AIAA Student Member
†Assistant Professor, Aerospace Engineering, 229 Hammond Building, AIAA Member

$\vec{U}$ = local relative velocity
U = local relative velocity magnitude
$\vec{v_i}$ = local inflow velocity
α = angle of attack
θ = local airfoil pitch angle
μ = dynamic viscosity
ν = kinematic viscosity
ρ = undisturbed air density
ϕ = inflow angle
$\vec{\omega}$ = rotor angular velocity
ω = rotor angular speed

II. Introduction

The design of rotary-wing aircraft is a complex problem, encompassing a wide range of interdisciplinary engineering design problems coupled together to achieve a common goal; an aerial vehicle that can take off and land vertically. One of the more complex elements of such a vehicle is the aerodynamic design of the rotor, or rotors, which allow it to generate forces and moments for the purposes of lift, propulsion, and control. While many theoretical and empirical models exist to predict the performance of such a system, they are somewhat limited due to their approximate nature and inherent assumptions. No analytical model exists that can reliably predict the performance, or wake structure of a rotor under all possible operating conditions with a high degree of absolute accuracy. Experimental testing of such rotors is often prohibitively expensive, due to the sheer scale of models and experimental facilities required, and the potential need for design iteration; changes to the rotor design require fabricating a new model to test. High-fidelity computational models, including large eddy simulations and direct numerical simulations, can be just as expensive with the computational resources available today, and in the foreseeable future. This is particularly true when considering the design of new types of electric vertical takeoff and landing (eVTOL) vehicles, which tend to contain multiple rotors in a variety of configurations. At the larger end of the spectrum, such vehicles tend to fall in the broader scope of UAM, as they are designed for personnel transport, and require large rotor systems to operate effectively. Throughout the vehicle's operating envelope, the rotors can often interact with each other in different ways; during takeoff and landing they may resemble a tandem configuration, but in forward-flight the rotors may be arranged closer to a coaxial layout. The way one rotor's wake interacts with the others can change dramatically depending on the given flight condition, leading to incredibly complex aerodynamic phenomena which can be difficult to model or predict accurately. Being able to accurately replicate these types of conditions using small-scale models can allow for high-fidelity measurements of the wake dynamics in such systems with significantly lower cost than a full-scale experimental study, and better representation of the real-world physics than any computational model.

There are currently a plethora of UAM vehicle configurations being developed and tested, but most tend to fall into one of four major categories: multirotor, lift + cruise, tiltrotor, and tiltwing. Multirotor vehicles consist of a series of rotors, oriented such that the thrust direction is vertical, which typically have individual collective pitch and speed control, providing the lift and control forces required for flight. The lift + cruise configuration similarly has a series of vertically-oriented rotors, with the addition of a propeller to provide forward thrust, and often wings to produce additional lift during forward-flight, augmenting the thrust produced by the main rotors. The tiltrotor concept again contains a series of rotors to allow for vertical takeoff and landing (VTOL) capability, which can then tilt into a propeller configuration to produce forward thrust, leaving the wings to generate most of the required lift. Finally, the tiltwing concept is similar in principle to the tiltrotor, but the rotors are mounted directly to the vehicle's wings, which all tilt as a single unit to allow for the transition between VTOL and forward-flight. The key commonality between all these vehicle concepts is the presence of a series of rotors operating in close proximity, over a wide range of flight conditions. This brings about the potential for complex interactional aerodynamic effects which have not been studied in nearly as much detail as conventional helicopter or fixed-wing aircraft configurations [1–3].

It is common practice when experimentally studying the aerodynamics of an engineering system to use scaled-down models which are geometrically similar to the objects they represent; this can minimize the required size of the testing facility, such as a wind tunnel, though there are challenges in doing so for rotorcraft applications. In order to accurately reproduce the rotor's operating conditions with an experimental model, the Mach number and Reynolds number along the blade must be matched as closely as possible to the full-scale operating conditions. Mach number is particularly important in the study of rotorcraft blades due to the compressible nature of the relevant aerodynamics, with blade

section velocities often reaching high-subsonic or even transonic conditions. This is especially true when the noise produced by the rotor is of interest to the experiments [4]. In practice this limits the minimum model scale that can practically be used in an experiment. While adjusting conditions to maintain a constant tip Mach number, the Reynolds number will continue to decrease as the rotor is scaled down, eventually reaching a point where the aerodynamics do not reflect the full-scale conditions and no meaningful correlation can be made with the data. Experiments have shown that in the case of typical helicopter rotors, scaled models can be used down to $1/7^{\text{th}}$ of the full scale, while still providing representative acoustic data [4]. However, it has been found in other studies of helicopter noise that at $1/7^{\text{th}}$ scale, there can be significant differences in noise produced by Blade-Vortex Interaction (BVI) resulting from changes in rotor aerodynamic behavior, depending on the rotor operating conditions. The significant decrease in Reynolds number is cited as a contributing cause to this discrepancy [5]. There is a strong link between Reynolds number and certain aerodynamic phenomena which contribute to BVI noise, including boundary layer thickness, and tip vortex strength, both of which are critical to capturing the behavior of the rotor wake [6]. If detailed data on the structure of the rotor wake and behavior of shed vortices is desired, Reynolds number is clearly an important factor to consider. Ideally both the Reynolds number and Mach number, as defined in Eqns. 1 and 2 are matched simultaneously:

$$Re = \frac{\rho U c}{\mu} \tag{1}$$

$$M = \frac{U}{a} \tag{2}$$

$$Re = \frac{\rho M a c}{\mu} \tag{3}$$

If the Mach number is matched on the model, then the fluid properties, either density, viscosity, or sound speed, must be altered in order to achieve the same Reynolds number as full-scale, as is shown by Eq. 3. This indicates that scale model tests of rotors in ambient air will always operate at reduced Reynolds numbers if the same geometry is used as full-scale. Past work has used working fluids with different kinematic viscosities than air ($\nu = \mu/\rho$), particularly R-12, for small-scale rotorcraft testing with good success [7]. Compressed air offers an attractive alternative to this method because the density is nearly linearly proportional to the pressure, while both the sonic velocity and dynamic viscosity are only a weak function of pressure. This means that both Reynolds number and Mach number can be matched to full-scale conditions on small models using compressed air. Compressed air presents other practical attributes over the use of other heavy gasses such as the low-cost, ease of availability, and reduced safety concerns compared to refrigerants or other heavy gasses (no risk of suffocation or toxicity in the event of a leak). Furthermore, the handling and recovery after use of the specialized gasses can be avoided.

III. Theoretical Background

A. Airfoil Performance Trends

An airfoil's performance characteristics can vary significantly with changes in Reynolds number, as is visible in the plot of the dependence of an airfoil's efficiency on Reynolds number and α, shown in Fig. 1. C_l typically has a linear dependence on α so long as the flow remains attached. Once the boundary layer begins to separate from the airfoil surface, a sharp drop in C_l is observed as the separated flow on the upper surface of the airfoil results in a significantly higher surface pressure in this region, reducing lift [8]. For low Reynolds numbers, the flow over the airfoil can be entirely laminar, leading to the increased likelihood of a laminar separation region. At higher Reynolds numbers, the boundary layer transitions to turbulent part of the way along the airfoil surface, making the flow more resistant to separation. As Reynolds number increases, the stall point becomes delayed to higher α, as is expected [8]. Given this trend, it is expected that for low angles of attack while the flow remains attached, the Reynolds number dependence of C_l/C_d shown in Fig. 1 is mainly due to a decrease in C_d as Reynolds number increases.

The dependence of C_d on Reynolds number can be explained by the competing effects of laminar boundary layer separation and transition to turbulence. For lower Reynolds numbers, the flow remains mostly laminar and therefore is not able to reattach after separating, resulting in a rapid increase in drag with further increases in angle of attack [9]. For higher Reynolds numbers, laminar separation causes the flow to transition from laminar to turbulent off the airfoil surface, aiding in reattachment further downstream on the airfoil, as turbulent mixing brings higher momentum fluid into the boundary layer [9]. This process is known as a Laminar Separation Bubble (LSB), and generally enables higher

lift to be maintained at larger angles of attack, but also increases drag due to the presence of turbulence in the boundary layer, and the large, low-pressure region inside the LSB [9–11]. For high enough Reynolds numbers, the boundary layer will transition to turbulent before separation occurs, causing drag to increase without a significant effect on lift [12]. This results in a change in the shape of the entire C_d curve, significantly altering the drag performance of the airfoil. These phenomena have been outlined as the reason why airfoils designed for large vehicles such as commercial airliners perform poorly when applied to smaller vehicles at lower Reynolds numbers, illustrating the need for careful consideration of airfoil section geometry on model behavior at low Reynolds numbers [12–14]. Knowing this dependence of airfoil performance on Reynolds number, it cannot be reasonable to expect geometrically similar small-scale models to behave identically to their full-scale counterparts, so long as the Reynolds number difference is great enough that the flow kinematics do not exhibit the same behavior. Previous studies on the scaling of wind turbine performance have shown a general stabilization of performance coefficients as the Reynolds number passes some critical value, which is a function of the airfoil geometry being used [15]. If the full scale rotor conditions are beyond this critical Reynolds number, the experimental model must be operating within that same regime, but exact matching of Reynolds number is not necessary to achieve the same performance characteristics. If the conditions of interest are in the regime in which performance coefficients are a function of Reynolds number, care must be taken to design the experiments to replicate full-scale conditions as accurately as possible to produce data which is physically meaningful with reference to the full-scale geometry.

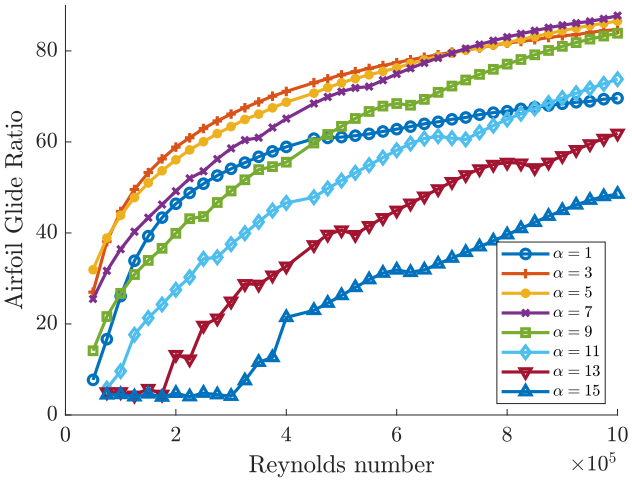

Fig. 1 Glide ratio, or the ratio of C_l/C_d, for the airfoil section at the 75% radial station of the rotor being investigated, as a function of Reynolds number and α.

B. Blade Element Theory Analysis

With this Reynolds number-dependence of airfoil performance in mind, the principles of Blade Element Theory (BET) can be used to analyze the effects on rotorcraft performance. For the sake of simplicity, it is assumed that each annulus of the rotor disk behaves independently of any other, such that 3D effects are negligible and each airfoil section along the blade can be treated as an independent, quasi-2D airfoil. The relative velocity observed by a given blade element can be computed based on the rotational speed of the rotor, radial position of the element, and induced inflow velocity. The local angle of attack can then be determined based on the local airfoil pitch and inflow angles. The result is an aerodynamic force which can be decomposed into lift and drag, as defined in Eqs. 4 and 5, which are normal to and aligned with the relative velocity, respectively. The local lift and drag forces can then be transformed into global rotor plane thrust, torque and power, as defined in Eqs. 6 to 8.

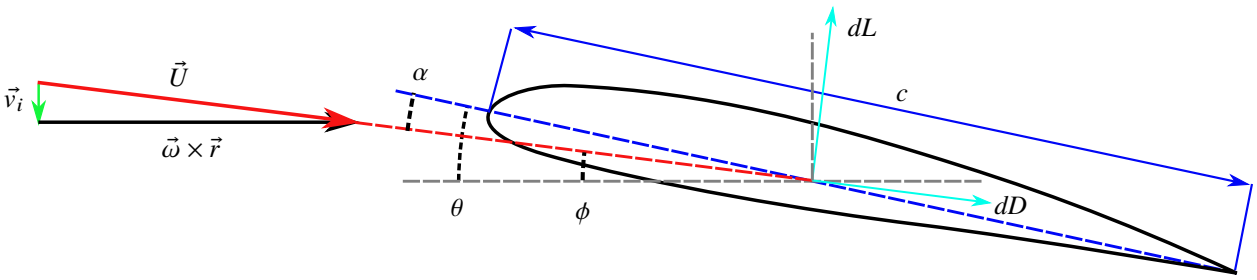

Fig. 2 Schematic showing relevant velocity components and angles on a typical rotor blade element.

$$dL = \frac{1}{2} C_l \rho U^2 c \Delta r \tag{4}$$

$$dD = \frac{1}{2} C_l \rho U^2 c \Delta r \tag{5}$$

$$dT = \frac{1}{2} (C_l \cos\phi - C_d \sin\phi) \rho U^2 c \Delta r \tag{6}$$

$$dQ = \frac{1}{2} (C_l \sin\phi + C_d \cos\phi) \rho U^2 c \Delta r \tag{7}$$

$$dP = \frac{1}{2} \omega r (C_l \sin\phi + C_d \cos\phi) \rho U^2 c \Delta r \tag{8}$$

The total resultant force, torque and power are the summation of the above expressions over each of the rotor blades. Both thrust and power are dependent on C_l and C_d, which are in general a function of the angle of attack and the Reynolds number. Provided the flow over the airfoil section is not separated and $\vec{v}_i$, and therefore α, are relatively constant, little to no variation in C_l will be observed. C_d however, can change considerably as Reynolds number varies. In the above expression for dT, the lift term contains the cosine of ϕ, whereas the drag term contains the sine of ϕ. This angle is typically not large, resulting in the lift term dominating the total rotor thrust expression. As C_l does not change with Reynolds number for an unseparated airfoil, it is predicted that the thrust produced by a rotor should not change appreciably with Reynolds number. In the expression for P however, the relative importance is reversed. The drag term now contains the cosine of ϕ, and C_d for a given angle of attack can vary considerably, even for an unseparated airfoil. It is therefore predicted that for a rotor with mostly attached flow over the lifting surfaces, as Reynolds number is varied the overall C_T of the rotor should not change significantly, while the C_P will. However, if the flow is separated over part of the rotor during operation, changes in both C_T and C_P will be observed.

IV. Experiments

The new compressed air wind tunnel (CAWT) at the Pennsylvania State University, shown in Fig. 3, was designed explicitly for the purpose of scale-matched aerodynamic testing using high density air, primarily consisting of a circular pressure vessel with an internal diameter of 1.07 m, and a section which expands to a diameter of 2.4 m. The CAWT can withstand internal pressures of up to 34 atm, corresponding to an increase in Reynolds number of 34 times that at atmospheric conditions for a given experimental model. The large diameter section, which serves as the flow conditioning section when the CAWT is being used as a wind tunnel, has instead been used for this study as a static testing chamber for a rotor in hover. No mean flow was produced by the wind tunnel for these tests, with the rotor effectively in a hover configuration. Within the chamber, a test stand was installed to operate and instrument the rotor. The stand includes a KDE Direct 8218XF-120 brushless motor, an ATI Delta 6-axis load cell which resolves all six

Fig. 3 The Compressed Air Wind Tunnel (CAWT), a low-speed, closed-loop wind tunnel in which the internal ambient pressure can be raised to 34 atmospheres.

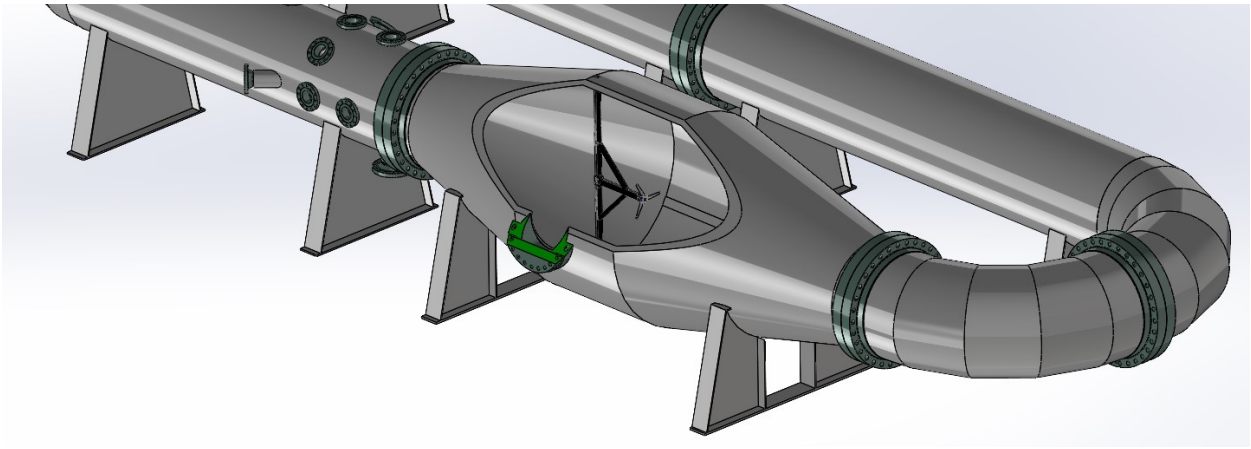

Fig. 4 Rendering of the CAWT, with a cross-sectional view exposing the rotor stand within the 2.4 m diameter chamber.

force and moment components, and a suite of other instrumentation to determine the operating conditions within the CAWT, including a pressure transducer, temperature probe, accelerometer, and infrared-tachometer. The experimental facility is shown schematically in Fig. 4.

A. Rotor Model

The rotor used in this study consists of a generic geometry provided by Joby Aviation which is representative of the types of blades commonly found on UAM vehicle concepts. Two variations of the small-scale rotor were fabricated. The first consisted of 3D printed blades mounted on a variable-pitch rotor hub and was used for preliminary testing at atmospheric pressure to verify the new facility's performance against an existing rotor testing stand. This rotor will also be useful for initial low-pressure experiments to identify specific test points of interest, which can then be studied in more detail in high-pressure. A stainless-steel fixed-pitch rotor was also designed and constructed to withstand the increased aerodynamic loads at the high-density conditions, and is shown in Fig. 5. The steel rotor was fabricated with a collective pitch angle of 15°, as defined by the blade pitch at the 75% radial station. The small-scale rotors are scaled down by a factor of 8 compared to the full-scale rotor, while maintaining the same geometry and proportions. The full scale rotor has a radius of $R = 2.90$ m, while the small-scale rotor has a radius of $R = 0.18$ m. To counteract the decrease in scale, the density of the air must be increased by a factor of 8 to match both Reynolds number and Mach number.

Fig. 5 The small-scale, fixed-pitch UAM rotor used to collect data for high Reynolds numbers in the CAWT.

B. Procedure

Thrust and torque measurements were taken over a range conditions typical of a subset of a UAM vehicle's operating envelope. Rotor speed was varied from 1000 to 5000 rpm, corresponding to the Mach number range of 0.05 to 0.27, as observed from 125 to 625 rpm on the full-scale rotor. By remaining below $M = 0.3$, compressibility effects can be assumed to be negligible, meaning there should not be a strong variation in rotor performance with Mach number. The pressure in the chamber was varied from atmospheric pressure up to 8.5 atm, corresponding to densities from 1.2 kg/m^3 to 10.2 kg/m^3, to go slightly beyond what was required to match the full scale Reynolds number, and to investigate the variation in rotor performance over a range from model-scale through full-scale conditions. At each ambient density, the rotor was brought through a full sweep of speeds, in order to characterize its performance as conditions varied.

Each data point is obtained from a time average of a 20 s long sample of the forces, moments, and rotor speed. The density for each condition is calculated from the measured pressure and temperature of the air in the chamber, taking into account real-gas effects [15].

V. Results

Presented in Figs. 6 and 7 are the experimental data outlining the performance of the rotor over a range of ambient densities. The data are plotted dimensionally in Figs. 6a and 6b, showing the trend of total thrust and power as functions of rotational speed, and ambient pressure, or density. The line colors in Figs. 6a and 6b correspond to the different ambient pressures, ranging from 1 atm to 8.5 atm, as indicated by the labels. The general trend in the data shows that thrust varies quadratically with rotational speed whereas power varies cubically, which is typical for rotorcraft.

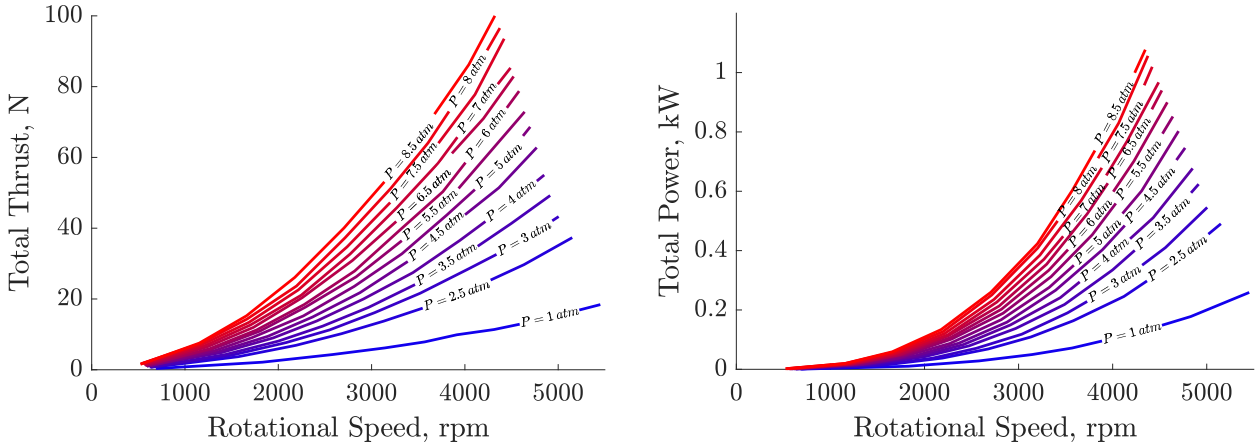

(a) Total rotor thrust. **(b) Total rotor power.**

Fig. 6 Total rotor performance characteristics measured as a function of rotational speed and background static pressure. Static pressure ranges from ambient (1 atmosphere) up to 8.5 atmospheres.

Rotor performance is often specified in terms of nondimensional coefficients, including the thrust coefficent C_T, and power coefficient, C_P, the definitions for which, shown in Eqs. 9, and 10 respectively, allude to these nonlinear dependencies on rotor speed. C_T contains the term ω^{-2}, and C_P contains the term ω^{-3}, which result in dimensionless coefficients which remain approximately constant over a range of rotor speeds. The data are then plotted in a nondimensional form using these coefficients in Figs. 7a and 7b, to better analyze the scaling behavior. Each colored line represents the variation in performance, as a function of Reynolds number at the 75% radial station, while the blade tip Mach number is held constant.

$$C_T = \frac{T}{\frac{1}{2}\rho A \omega^2 R^2} \tag{9}$$

$$C_P = \frac{P}{\frac{1}{2}\rho A \omega^3 R^3} \tag{10}$$

The data show that the performance of the rotor, in particular C_P, is a function of Reynolds number. As Reynolds number increases, C_P shows a nonlinear trend, initially decreasing before reaching a minimum and starting to increase again at higher Reynolds numbers. The trend in thrust displays a similar overall shape, but with a smaller relative variation, indicating C_T is not as strongly affected by Reynolds number in comparison to C_P. For decreasing Reynolds numbers below 150,000, C_P increases rapidly, which matches the trends seen in several other studies which analyze the performance of small-scale rotors and propellers [12–14]. This trend is further backed up by an examination of the glide ratio for the airfoil at the 75% radial station, together with the earlier discussion on BET. As shown previously in Fig. 1, the glide ratio, which is a representation of an airfoil's efficiency to generate lift while producing minimal drag, generally increases with Reynolds number, and is also a strong function of α, particularly for higher angles of attack where the flow separates. Although the airfoil section does vary along the span of the blade, the majority of the outboard

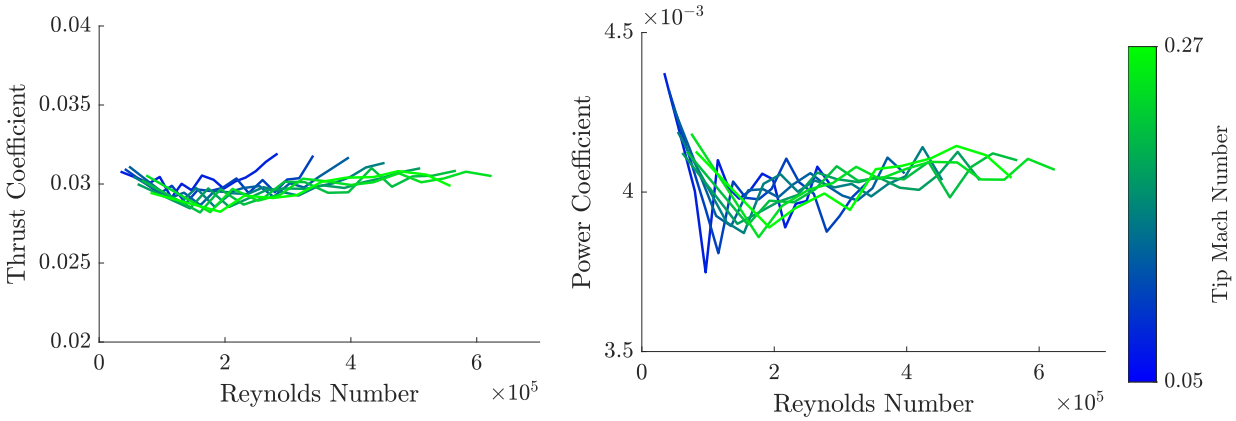

(a) Total rotor thrust coefficient.

(b) Total rotor power coefficient.

Fig. 7 Total rotor performance coefficients measured as a function of Reynolds number and blade tip Mach number. Mach number varies from 0.05 up to 0.27.

section closely resembles the element at the 75% radial station, on which the data presented in Fig. 1 is based. From the earlier discussion of rotor performance based on a BET analysis, the variation in C_T is linked to the boundary layer separation present along the blade, as it would be expected to remain constant if the boundary layer did not separate.

The blade pitch at the 75% radial station is 15°, meaning the angle of attack is slightly below this value due to the effects of $\vec{v}_i$. The exact values of α are not known, due to the lack of inflow data available for the rotor, however it can be predicted to be relatively close to the blade pitch under the assumption that the magnitude of the component of velocity from the rotor's rotation, $\vec{\omega} \times \vec{r}$, is significantly larger than $\vec{v}_i$. From the airfoil data presented in Fig. 1, the effects of boundary layer separation can be observed at values of α as low as 7°, so it can be assumed that the boundary layer over this particular blade element is separated. Further outboard, the blade pitch decreases, reducing the value of α enough that the boundary layer is no longer separated. For the more inboard sections of the rotor, the airfoil geometry changes significantly, meaning Fig. 1 is no longer a valid approximation. However, the pitch angle further increases leading to even higher values of α, meaning the boundary layer is likely separated for most of the inboard section at this collective pitch angle. Therefore, the severity of the separated boundary layer's impact on airfoil performance, and the spanwise region of the blade affected, are functions of Reynolds number as indicated by Fig. 1. The inboard section of the rotor's contribution to overall rotor C_T and C_P is relatively small compared to that of the outboard section, due to the lower relative velocities seen by the blade elements in this region. As the Reynolds number increases, more of the separated flow is able to reattach, increasing the overall C_T. This explains the slight increase in C_T observed over the range of $Re = 200,000$ to $Re = 600,000$. In addition, there doesn't appear to be any Mach number dependence of the rotor performance, a trend which is clearly visible in Figs. 7a and 7b. All of the lines, which each represent a constant Mach number, collapse into the same region. This was to be expected due to the present study only examining the incompressible regime, with $M < 0.3$ over the entire range of experiments.

VI. Conclusion

This study presents a novel method for obtaining scale-matched performance data of rotorcraft blades, by using compressed air to achieve the densities required to match the Reynolds number and Mach number simultaneously. The data displays a nonlinear trend in C_P with varying Reynolds number, indicating that the types of airfoils used on UAM rotors are sensitive to changes in Reynolds number, and illustrates the need to accurately replicate full scale conditions in an experimental model. It is expected that the performance of the rotor would eventually stabilize for higher Reynolds numbers, based on similar scaling experiments on wind turbine rotors, and airfoil behavior [12, 15]. The variation in airfoil performance with Reynolds number observed in the present study correlated well with general trends seen in existing literature for similar conditions [1, 2, 13, 14]. At these low Reynolds numbers, significant changes in airfoil performance with varying Reynolds number have been observed in a variety of studies [7, 12, 14, 15]. The trends in the data showed a significant change in C_P with Reynolds number, and a comparatively smaller change in C_T, which can be explained by the large region of the blades over which the boundary layer is separated. For lower blade collective

pitch angles, it is expected that the boundary layer would have remained attached over a larger portion of the blade span. This would result in a less significant dependence of C_T on Reynolds number, as C_l only varies with Reynolds number when the boundary layer is separated. Given the substantial portion of the blade span over which the boundary layer has separated, the collective pitch angle of 15° represents an operational edge-case, where changes to the rotor's control inputs may not have the desired effect, i.e., increasing pitch may result in decreased thrust due to boundary layer separation effects becoming more significant, as shown in the trends of Fig. 1. Accurate characterization of rotor performance at such conditions can be critical in optimizing a vehicle design for both performance and safety. This study provides an example of how the performance under these critical conditions can depend on Reynolds number, and demonstrates the applicability of hyperbaric testing conditions to characterize performance at full-scale Reynolds numbers at a fraction of the cost of a full-scale experiment.

The ability to acquire high-fidelity aerodynamic data using models which are a fraction of the size of the system of interest presents an attractive option to the designers of future rotorcraft, be they single rotor or multirotor vehicles. Much of the cost of an experimental campaign involves the fabrication of the experimental models to be used, as well as the operation of the testing facility. As the scale of experiments is brought down, so too is the cost of fabricating models, and the personnel required to operate the testing facilities. In addition, reducing the scale of experimental models better facilitates flow measurement and visualization techniques, since the scale of the area to be instrumented decreases as well. Testing in hyperbaric conditions therefore has the potential to make experimental studies much more cost effective and accessible, allowing experimentalists to cover a much broader testing envelope, and to more rapidly iterate designs and test conditions.

In the future, the scope of the present study will be expanded to include detailed measurements of the rotor wake, investigation of multirotor configurations, and acoustic measurements. The wake measurements will consist of hot-wire anemometry data to characterize the wake structure and turbulence characteristics. A second rotor stand will also be developed for the CAWT, allowing for testing of multirotor systems, including coaxial and tandem layouts. The eventual goal will be to measure the interactional aerodynamic effects resulting from multiple rotors, and their wakes, being in close proximity to one another, and analyze the ability to accurately characterize these phenomena using small-scale models in hyperbaric air.

Acknowledgments

The authors thank the Pennsylvania State University, the US Army, Navy, and NASA, for funding this research through the Vertical Lift Research Center of Excellence (VLRCOE) program, as well as all our technical points of contact for providing feedback and guidance. The authors would also like to thank Joby Aviation, for providing the rotor geometry used for these experiments.

References

[1] Garrow, L. A., German, B. J., and Leonard, C. E., "Urban Air Mobility: A Comprehensive Review and Comparative Analysis With Autonomous and Electric Ground Transportation for Informing Future Research," *Transportation Research Part C: Emerging Technologies*, Vol. 132, 2021. https://doi.org/10.1016/j.trc.2021.103377, URL https://www.sciencedirect.com/science/article/pii/S0968090X21003788.

[2] Silva, C., and Johnson, W., "VTOL Urban Air Mobility Concept Vehicles for Technology Development," *AIAA AVIATION Forum*, AIAA, 2018. https://doi.org/10.2514/6.2018-3847.

[3] Kadhiresan, A. R., and Duffy, M. J., "Conceptual Design and Mission Analysis for eVTOL Urban Air Mobility Flight Vehicle Configurations," *AIAA AVIATION Forum*, AIAA, 2019. https://doi.org/10.2514/6.2019-2873.

[4] Schmitz, F. H., Boxwell, D. A., Splettstoesser, W. R., and Schultz, K. J., "Model-Rotor High-Speed Impulsive Noise: Full-Scale Comparisons and Parametric Variations," *Vertica*, Vol. 8, No. 4, 1984, pp. 395, 422.

[5] Boxwell, D. A., Schmitz, F. H., Splettstoesser, W. R., and Schultz, K. J., "Helicopter Model Rotor-Blade Vortex Interaction Impulsive Noise: Scalability and Parametric Variations," *Journal of the American Helicopter Society*, 1987.

[6] Schmitz, F. H., and Yu, Y. H., "Helicopter Impulsive Noise: Theoretical and Experimental Status," *Journal of Sound and Vibration*, Vol. 109, 1986, pp. 361, 422.

[7] Singleton, J. D., and Yeager Jr, W. T., "Important Scaling Parameters for Testing Model-Scale Helicopter Rotors," *Journal of Aircraft*, Vol. 37, No. 3, 2000, pp. 396, 402.

[8] Sengupta, T. K., *Theoretical and Computational Aerodynamics*, Wiley, 2015.

[9] Schmidt, G. S., and Mueller, T. J., "Analysis of Low Reynolds Number Separation Bubbles Using Semiempirical Methods," *AIAA journal*, Vol. 27, No. 8, 1989, pp. 993–1001.

[10] Dini, P., and Maughmer, M. D., "Locally Interactive Laminar Separation Bubble Mode," *Journal of aircraft*, Vol. 31, No. 4, 1994, pp. 802–810.

[11] O'Meara, M., and Mueller, T. J., "Laminar Separation Bubble Characteristics on an Airfoil at Low Reynolds Numbers," *AIAA journal*, Vol. 25, No. 8, 1987, pp. 1033–1041.

[12] Mueller, T. J., and DeLaurier, J. D., "Aerodynamics of Small Vehicles," *Annual Review of Fluid Mechanics*, Vol. 35, 2003, pp. 89, 111. https://doi.org/10.1146/annurev.fluid.35.101101.161102.

[13] Simmons, B. M., and Hatke, D. B., "Investigation of High Incidence Angle Propeller Aerodynamics for Subscale eVTOL Aircraft," Tech. rep., NASA Langley Research Center, 04 2021.

[14] Deters, R. W., Ananda, G. K., and Selig, M. S., "Reynolds Number Effects on the Performance of Small-Scale Propellers," *AIAA AVIATION Forum*, AIAA, 2014. https://doi.org/10.2514/6.2014-2151.

[15] Miller, M. A., Kiefer, J., Westergaard, C., Hansen, M. O. L., and Hultmark, M., "Horizontal Axis Wind Turbine Testing at High Reynolds Numbers," *Phys. Rev. Fluids*, Vol. 4, 2019, p. 110504. https://doi.org/10.1103/PhysRevFluids.4.110504.